OPTICS

Tip-enhanced strong coupling spectroscopy, imaging, and control of a single quantum emitter

Kyoung-Duck Park[1,2]*†, Molly A. May[1]*, Haixu Leng[3], Jiarong Wang[1], Jaron A. Kropp[3], Theodosia Gougousi[3], Matthew Pelton[3]†, Markus B. Raschke[1]†

Optical cavities can enhance and control light-matter interactions. This level of control has recently been extended to the nanoscale with single emitter strong coupling even at room temperature using plasmonic nanostructures. However, emitters in static geometries, limit the ability to tune the coupling strength or to couple different emitters to the same cavity. Here, we present tip-enhanced strong coupling (TESC) with a nanocavity formed between a scanning plasmonic antenna tip and the substrate. By reversibly and dynamically addressing single quantum dots, we observe mode splitting up to 160 meV and anticrossing over a detuning range of ~100 meV, and with subnanometer precision over the deep subdiffraction-limited mode volume. Thus, TESC enables previously inaccessible control over emitter-nanocavity coupling and mode volume based on near-field microscopy. This opens pathways to induce, probe, and control single-emitter plasmon hybrid quantum states for applications from optoelectronics to quantum information science at room temperature.

INTRODUCTION

Single quantum emitters in solids in the form of quantum dots (QDs), nitrogen vacancy centers, or engineered defects as artificial atoms have emerged as promising platforms for quantum sensing, metrology, and information processing (1–4). These quantum emitters can now be controlled using optical cavities to enhance the coupling strength g between emitters and cavity photons to the point where it exceeds the rates of quantum decoherence in the system. However, the diffraction limit restricts the mode volume V and thus the coupling strength $g \propto 1/\sqrt{V}$, which has so far required operation at cryogenic temperatures to overcome decoherence (5–9).

As an alternative approach, plasmonic cavities with nanoscale mode volumes provide a promising platform for ultracompact cavity quantum electrodynamics (cQED) systems even at room temperature (10–20). Specifically, QDs or molecules coupled strongly to plasmonic nanocavities give rise to a plexcitonic state as a hybrid state of a plasmon and an exciton (21).

The observation of these plexcitonic states from single emitters was recently demonstrated with Rabi splitting in scattering spectra (16, 18) even at room temperature. However, in contrast to photoluminescence (PL), the discrimination of strong coupling from competing Fano-like interference effects can still be ambiguous in scattering (22). In addition, once fabricated, the static QD nanocavity devices constrain tunability and control. Furthermore, because of their nanoscopic dimensions, the details of field confinement in these structures are not accessible to conventional microscopy. This limits the ability to measure, optimize, and control coupling and dissipation. Therefore, to expand the utility of this nanocavity approach, a nanoimaging-based implementation of plasmonic strong coupling is desired.

Here, we demonstrate tip-enhanced strong coupling (TESC) spectroscopy, imaging, and control based on scanning probe microscopy. A resonant plasmonic cavity with nanoscale mode volume of $V/\lambda^3 \leq 10^{-6}$

is deterministically formed between a nano-optical antenna tip and a metal mirror substrate. Using this approach, we scan, locally address, and probe single QDs at room temperature, achieving clear, high-contrast plexcitonic PL with Rabi splitting up to 163 meV. We probe different QDs with exciton energies detuned from the plasmonic cavity over a range of ~100 meV, thereby demonstrating anticrossing of the upper and lower polariton modes. In addition, on the basis of the precise subnanometer distance control of the tip, we spatially map and reversibly modulate the coupling strength over a range of up to 140 meV.

This work extends a previous approach based on an engineered slot antenna on a tip to achieve strong coupling of single QDs near the slot (23). However, the slot antenna limits the cavity mode volume and spatial resolution that can be obtained. Instead, in TESC, we use the inverse structure of a conical optical antenna nanotip to form a nanocavity between the tip and a metal mirror substrate. This eliminates the need to generate a nanogap on the tip itself (Fig. 1) and provides for a greatly simplified and generalizable approach for active control of the confined nanocavity field over distances down to the atomic scale. The resulting improved signal quality and contrast in TESC with unambiguous two-peak splitting, anticrossing, and dynamical subnanometer control over interactions between a nanocavity and a single quantum emitter enables new methods to measure and control quantum state transfer, light-matter entanglement, and single-photon quantum gates.

TESC corresponds to a new paradigm of near-field optical microscopy. While previous near-field optical microscopy efforts have generally focused on a minimally invasive tip-sample interaction to obtain an unperturbed spectroscopic signature (24), TESC moves from a traditionally nonperturbative to a strongly perturbative regime in which the tip acts as a nanocavity to induce, probe, and control quantum hybrid states for all-optical room temperature quantum metrology and sensing at the nanoscale.

TESC is the optical analog to recent advances in scanning tunneling microscopy based on strongly perturbing tip-induced electric or spin interactions to induce and probe previously unobserved quantum magnetic or quantum coherence effects in a localized and tunable fashion (25–27).

RESULTS

As the quantum emitter, we use single isolated CdSe/ZnS QDs, which are drop-cast onto a flat, template-stripped Au surface that is coated

[1]Department of Physics, Department of Chemistry, and JILA, University of Colorado, Boulder, CO 80309, USA. [2]Department of Physics, Ulsan National Institute of Science and Technology (UNIST), Ulsan 44919, Korea. [3]Department of Physics, University of Maryland, Baltimore County, Baltimore, MD 21250, USA.
*These authors contributed equally to this work.
†Corresponding author. Email: markus.raschke@colorado.edu (M.B.R.); mpelton@umbc.edu (M.P.); kyoungduck.park@colorado.edu (K.-D.P.)
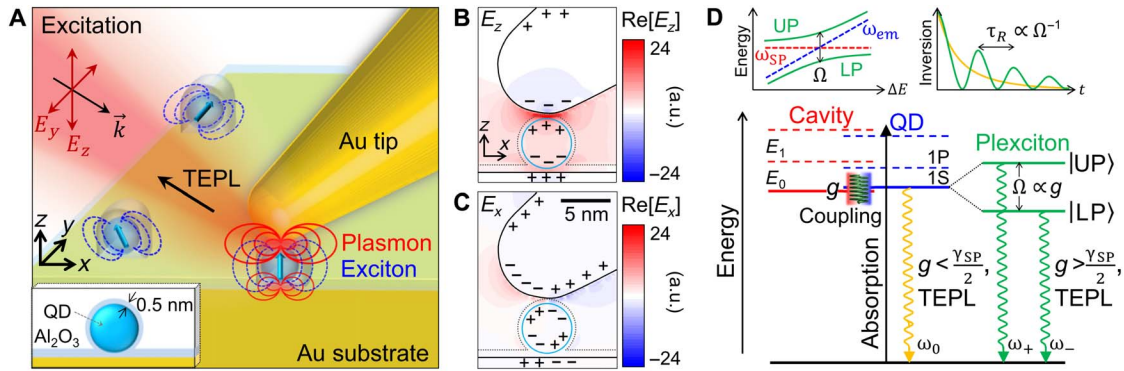
Fig. 1. TESC spectroscopy and energy diagram for the plasmon and exciton in the weak and strong coupling regime. (**A**) The strongly confined $|E_z|$ fields in a single isolated QD (CdSe/ZnS) with a 0.5-nm dielectric capping layer (Al_2O_3) and a tilted Au tip induce coupling between the plasmon and exciton. Simulated out-of-plane (**B**) and in-plane (**C**) optical field distributions in the plasmonic cavity shown in (A). a.u., arbitrary units. (**D**) Energy diagram for the plasmonic cavity (red), QD (blue), and upper and lower polariton states (green) with PL energy in the weak (orange) and strong (green) coupling regimes. When the coupling exceeds system losses, the split polariton states emerge and the system begins to undergo Rabi splittings and Rabi oscillations, as illustrated above.

with a thin Al_2O_3 layer. The QDs are protected against photo-oxidation by another ultrathin 0.5-nm Al_2O_3 capping layer and are characterized by atomic force microscopy (AFM) to confirm even dispersion of the particles (section S1 and fig. S1). The plasmonic Au tips are etched electrochemically (28). Tip-enhanced photoluminescence (TEPL) spectra are recorded under continuous-wave (632.8 nm, ≤1 mW) resonant tip–surface plasmon polariton (SPP) and QD-exciton excitation, as illustrated in Fig. 1A (for details, see Methods). The tilted tip (35° with respect to the sample surface in this case) controls the tip-SPP resonance frequency and maximizes the field enhancement, as shown recently (29). In the resulting plasmonic cavity, the corresponding SPP mode is most strongly bound in $|E_z|$, as confirmed by finite-difference time-domain (FDTD) simulations (Fig. 1, B and C). Sample scanning and tip-sample distance are controlled with ~0.2-nm precision using a shear-force AFM. All experiments are performed at room temperature.

Figure 1D shows a schematic energy diagram for the plasmon (red), exciton (blue), and their hybridized plexciton (green) with upper $|UP\rangle$ and lower polariton $|LP\rangle$ states. When the coupling strength g between the cavity plasmon and the QD exciton exceeds the SPP loss rate, γ_{SP}, i.e., $g > \frac{\gamma_{SP}}{2}$, quantum mixed states of the plexciton give rise to Rabi splitting in the TEPL spectra or, equivalently, a reversible Rabi oscillation between the plasmon and exciton. In contrast, in the weak coupling regime ($g < \frac{\gamma_{SP}}{2}$), the usual primarily radiative relaxation with enhanced PL intensity (orange) attributed to the plasmonic Purcell effect is observed at the exciton frequency (30).

We first characterize the emission properties of the uncoupled QD excitons in the far field, as shown by the PL spectrum (blue) in Fig. 2A. Independently, we characterize the tip surface nanocavity through its tip-SPP emission (31) (red), with the tip retracted to ~3 nm from a clean Au mirror substrate without QDs. From fitting to a Lorentzian line shape function, corresponding peak energies ($\omega_{QD} = 1.856$ eV and $\omega_{SP} = 1.912$ eV) and linewidths ($\gamma_{QD} = 0.097 \pm 0.002$ eV and $\gamma_{SP} = 0.126 \pm 0.002$ eV) are derived (section S2 and fig. S2). We note that ω_{SP} is expected to red-shift in the presence of the QD due to modification of the effective dielectric environment in the nanocavity (32). This is beneficial for increasing spectral overlap of SPP and QD resonances. We then scan and position the tip directly over an individual QD and measure its TEPL response coupled to the plasmonic cavity. In a series of experiments for different QDs with the same tip, we observe TEPL

spectra across a wide range of coupling strengths due to the random dipole orientation of the different QDs on the mirror substrate, as shown in Fig. 2A. Weak coupling leads only to enhanced PL with spectral broadening, with $\omega_{weak} = 1.860$ eV and $\gamma_{weak} = 0.118$ eV (orange), essentially identical to the unperturbed QD exciton peak. In contrast, in the strong coupling regime (green), for QDs with an out-of-plane transition dipole moment (TDM) with respect to the surface, a qualitatively different behavior with peak splitting and intensity enhancement is observed.

We fit the observed TEPL intensity spectra $I_{PL}(\omega)$ using a coupled harmonic oscillator model in the Weisskopf-Wigner approximation for an impulsively excited emitter, given by (33)

$$I_{PL}(\omega) =$$

$$\frac{\gamma_{QD}}{2\pi} \left| \frac{\gamma_{SP}/2 - i(\omega - \omega_{SP})}{\{(\gamma_{SP} + \gamma_{QD})/4 - i(\omega_{QD} - \omega_{SP})/2 - i(\omega - \omega_{QD})\}^2 + \Omega^2} \right|^2$$

(1)

Here, γ_{SP} and γ_{QD} are the decay rates; ω_{SP} and ω_{QD} are the resonance frequencies of the plasmon mode and QD, respectively; and Ω is the vacuum Rabi frequency (for details, see section S3). The corresponding coupling strength g can then be obtained from the fit parameters (section S4) as

$$g = 2\sqrt{\Omega^2 - \frac{(\omega_{QD} - \omega_{SP})^2}{4} + \frac{(\gamma_{SP} - \gamma_{QD})^2}{16}}$$

(2)

For the example shown in Fig. 2A, we obtain a coupling strength of $g \sim 143$ meV $> \frac{\gamma_{SP}}{2}$, i.e., well in the strong coupling regime. More extended theoretical models that take into account both plasmonic and QD losses reproduce the same spectral behavior of our experimental data (34, 35).

The Raman peak of Al_2O_3 ($\bar{\nu} = 1.897$ eV) observed in the far-field PL spectrum is not discernible in the TEPL spectra. This is because of the sparse distribution of QDs compared to the large area of Al_2O_3 coverage that contributes to the far-field signal.

Figure 2B (top) shows the PL evolution of the uncoupled QD, which exhibits the spectral diffusion and blinking behavior that are generally observed for different QDs. The plexciton TEPL spectra in
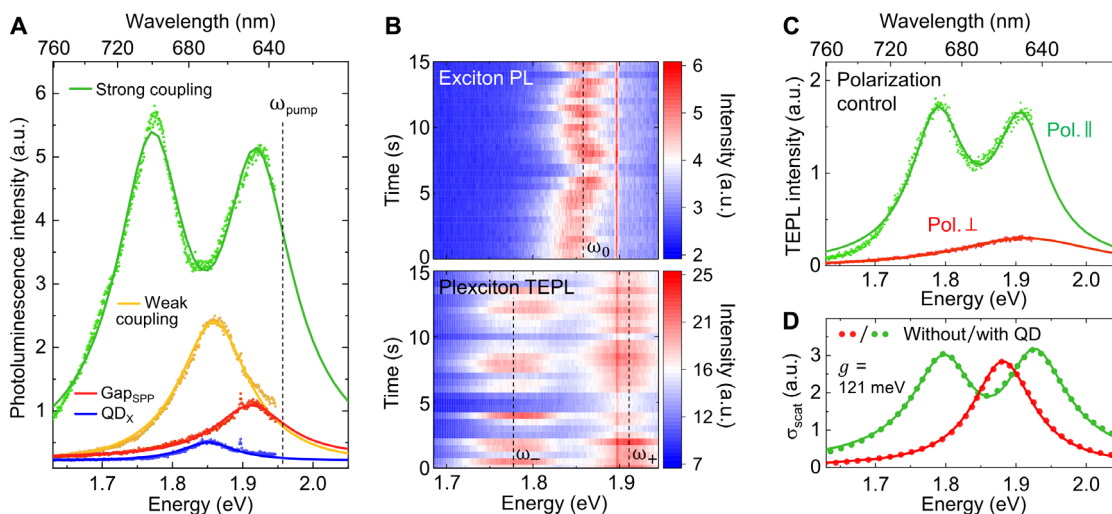
Fig. 2. Tip-enhanced plexciton PL at room temperature in the strong coupling regime. (**A**) PL spectra of the gap plasmon (red), QD exciton (blue), the weakly coupled plasmon-exciton mode (orange), and the strongly coupled plexciton mode (green). (**B**) PL evolution of the uncoupled (top) and the strongly coupled (bottom) single QD. (**C**) TEPL spectra for a polarization parallel (green) and perpendicular (red) with respect to the tip. (**D**) FEM simulation of scattering spectra for the plasmonic cavity without QD (red) and with a single QD (green). In (A), (C), and (D), the dots and lines indicate the measurement (or simulation) data and the corresponding model fits, respectively.

Fig. 2B (bottom) reveal a similar intensity fluctuation and no notable changes in coupling strength, which confirms that the tip-sample distance is precisely controlled in our experiments. In addition, the result shows that the typical blinking due to, e.g., nonradiative Auger recombination and/or thermalization processes (*36*) still occurs in the strong coupling regime.

As an important control experiment, we can vary the field enhancement in the $|E_z|$ direction through rotation of the incident laser polarization. For a QD with an out-of-plane TDM, for polarization parallel with respect to the tip axis, plexciton formation and emission (green) are induced, as shown in Fig. 2C. In contrast, for perpendicular polarization, only the tip plasmon PL is observed (red). This clear contrast concurs with three-dimensional (3D) FDTD simulations for the given experimental conditions, which show that the excitation polarization parallel with respect to the tip gives rise to an ~800-fold field intensity enhancement compared to polarization perpendicular with respect to the tip (see fig. S3), and which confirm the well-defined nature of the plasmonic nanocavity.

We next model the spectra and the observed Rabi splitting based on finite element method (FEM) calculations (*37*). In these models, the QD is treated as a dielectric nanoparticle with oscillator strength $f \sim 0.8$, a value that yields the best agreement with experimental observations (Fig. 2, A and C) and is consistent with recent work (*18*). Approximating the plasmonic antenna tip as a finite length ellipsoid, the resulting simulated scattering spectrum, as shown in Fig. 2D, exhibits the expected splitting of the hybridized state with $g \sim 121$ meV, in good agreement with the experiment (section S5).

As the tip interacts with different QDs in a large-area scan, we observe variations in plexciton coupling strength ranging from 70 meV (at the threshold for strong coupling) to 163 meV (well into the strong coupling regime), as shown in Fig. 3A. Because CdSe QDs have a TDM (μ_{QD}) oriented perpendicular to the crystallographic *c* axis of the nanocrystal (*38*), this variation can be described by the different orientations of QDs, which modify the coupling strength with the cavity $|E_z|$ field (*39*), given by $g \approx |\mu_{QD}||E_z|\cos\theta$, where θ denotes the angle between
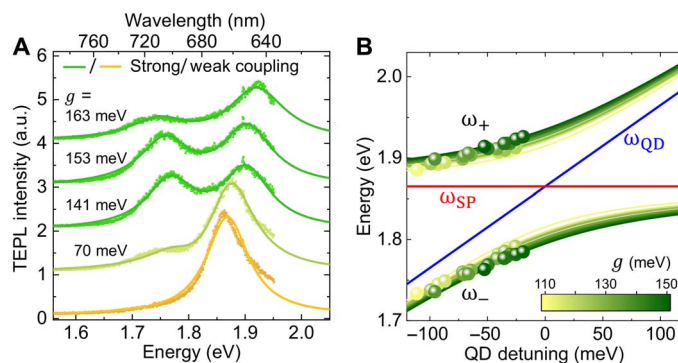

Fig. 3. TESC spectra with increasing coupling strength and plexciton energy diagram with QD detuning. (**A**) TEPL spectra of different single QDs with variation in coupling strength *g* and Rabi frequency. (**B**) Polariton energies from model fits (circles) and anticrossing curves from model calculations (lines) for each of the measured TEPL spectra of 21 different QDs. The expected surface plasmon (red) and QD (blue) detuning dependence is obtained from averaged values from the modeled 21 spectra.

the TDM and the surface normal. In addition to the QD orientation, the inevitable inhomogeneities in local QD environment, e.g., different Al_2O_3 layer thickness and roughness of the Au film, also give rise to variations in *g* values, but likely to a lesser degree.

In addition to the observed variation in coupling strength for different QDs, we also measure slightly different resonance frequencies for each QD due to variations in QD size and shape, which correspond to varying amount of spectral detuning from the plasmon resonance. Localizing 21 different QDs, we measure their TEPL spectra and determine the corresponding mode energies of the $|UP\rangle$ and $|LP\rangle$ branches and the QD energy detuning ($\omega_{SP} - \omega_{QD}$) by fitting to Eq. 1. With the nanocavity characterized by fixed $\omega_{SP} = 1.850$ eV and $\Gamma_{SP} = 0.160 \pm 0.010$ eV and identical for all QDs, and the narrow range of QD linewidth of $\Gamma_{QD} = 0.090 \pm 0.010$ eV for all QDs, the data can be

fit with the QD resonance frequencies ω_{QD} and the coupling strength g as the only free parameters (see section S4 for fitted values). The resulting dispersion of the $|UP\rangle$ and $|LP\rangle$ branches for each of the 21 QDs is plotted in Fig. 3B (circles) as a function of the detuning value, with color scale representing their corresponding g value obtained. A clear anticrossing is observed as shown in comparison with the expected cavity dispersion curve (red) and average QD energy (blue).

The data scatter in energy is caused by a variation in g from 107 to 152 meV. The corresponding set of plexciton energy dispersions calculated for each QD using eq. S1 (section S3) is shown in Fig. 3B as solid lines. This ability to measure individual QDs over a range of detuning values with a single plasmonic nanocavity demonstrates the distinct advantage of TESC spectroscopy.

In addition, TESC provides the ability to tune the coupling strength and control the nanocavity mode volume in interaction with an individual emitter. As an example, Fig. 4A shows the transition into the strong coupling regime with a steady increase in Rabi splitting up to $g \sim 140$ meV as we laterally scan the tip toward a QD over a length scale defined by the tip radius. Conversely, vertical tip-sample distance control with subnanometer precision shown in Fig. 4B reflects the extreme spatial confinement with decreasing gap width (40). The shorter length scale compared to lateral tip-QD separation is due to the rapid decrease in coupling strength g. Figure 4 (C and D) shows the corresponding tip-QD distance dependence of the coupling strength g and Rabi frequency Ω derived from Fig. 4 (A and B) (for details and corresponding values for ω_{SP} and ω_{QD}, see section S4). On the basis of these results, the optical mode volume V/λ^3 of the plasmonic nanocavity is esti-

mated to be $\leq 10^{-6}$, consistent with the expectation from the $|E_x|$ and $|E_z|$ field distribution calculation ($V \sim 10^3$ nm^3), as seen in Fig. 1 (B and C) and can readily be further reduced by using tips of smaller radius (41, 42).

In contrast to conventional cavities that interact in the far field, the presence of the emitter strongly modifies the mode volume, polarization distribution, and loss rate of a nano-optical cavity. While this complicates quantification and modeling of these properties, the emitter-cavity back-action provides previously unexplored control degrees of freedom, and scanning the nanocavity provides a way to determine its characteristics through TESC imaging.

DISCUSSION

In the following, we compare our result with recent studies on strong coupling of single emitters using plasmonic nanocavities. To date, most strong coupling studies have relied on multiple (n) emitters in the form of J-aggregates (43) to induce a large collective effect ($g \propto \sqrt{n/V}$). However, multiple emitters are impracticable for applications in quantum gates (44) and entanglement (45) because they exhibit an equidistant energy spectrum that is identical to a classical system. This means that the nonlinear optical properties of multiple emitters are qualitatively different than the single emitter case (46). However, the observation of peak splitting in scattering spectra from single emitters (16, 18) is not sufficient to ensure strong coupling, as other effects such as Fano-like interference can lead to nearly identical spectral features (22, 43). Probing strong coupling plexciton emission in the form of, e.g., PL of
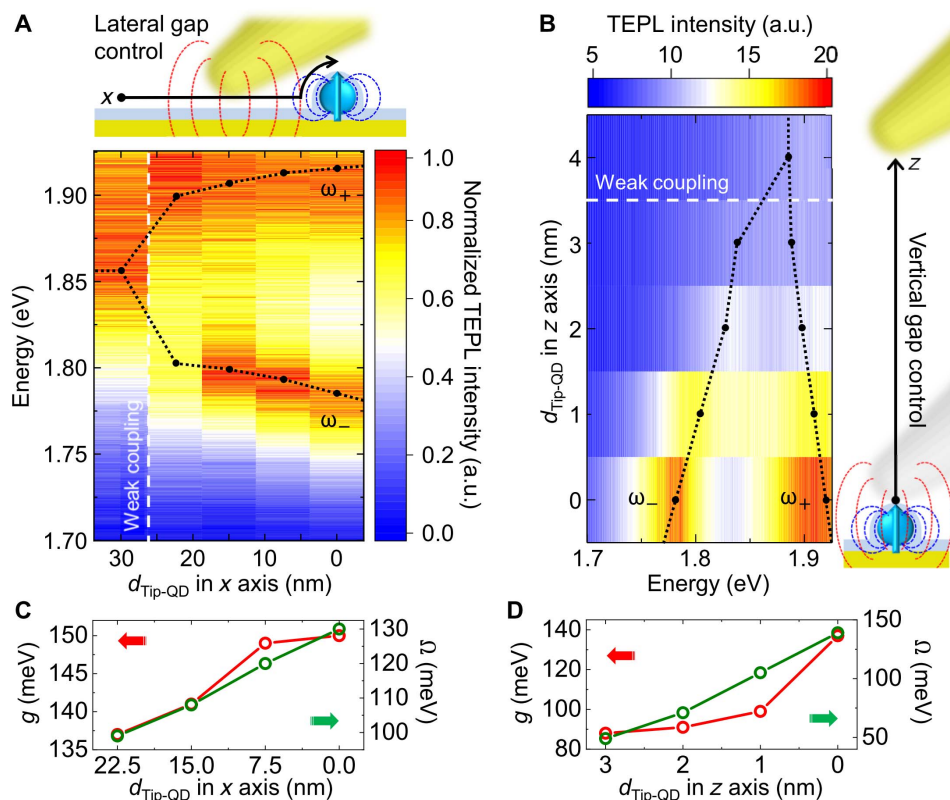

Fig. 4. Active control of tip-induced single QD strong coupling. TEPL spectra as the lateral (**A**) and vertical (**B**) tip-QD distances are varied from 30 to 0 nm and from 0 to 4 nm, respectively. (**C** and **D**) Coupling strength g and Rabi frequency Ω derived from model fit of the distance-dependent TEPL spectra from (A) and (B).

a single emitter overcomes these issues and provides unambiguous evidence of strong coupling for applications in quantum information and photonic quantum devices. However, the recent work using PL to probe strong coupling of a single QD coupled to a plasmonic slot structure (23) led to convoluted spectra with large background and competing interactions.

In contrast, our approach of TESC uses a combination of several enabling features that allow us to induce, image, and control single-emitter plexciton PL at room temperature with the following beneficial attributes. First, on the basis of the inverse geometry (47), instead of a nanogap in the tip itself, we induce the nanocavity between the tip and the sample, which provides tunable coupling and ultrasmall mode volumes (section S6). Second, with the tilted tip and thus spectrally controlled SPP, the field enhancement is further increased by suppressing the overdamped resonance of a conventional surface-normal oriented tip (29). Third, near-field coupling and polarization transfer to the tip with its few-femtosecond radiative lifetime (31) at the subnanometer gap between the tip and QD outcompetes the otherwise dominant nonradiative damping of a QD near a metallic surface (48).

CONCLUSION

Single emitters strongly coupled to nanophotonic modes are emerging as a promising enabling technology for nonlinear optics (49) and quantum information processing (50, 51) at the single-photon level. Our demonstration of TESC of single QD plexciton PL opens a new paradigm of perturbative near-field microscopy in the quantum limit that can be generalized to any optical modality. Specifically, the ability to rapidly and reversibly change the coupling strength through nanoscale tip positioning provides a new means of tuning these quantum-optical interfaces, providing a degree of functionality to control quantum dynamics. TESC can be extended further by using emitters with larger TDM, tips that provide smaller mode volume, and nanoplasmonic tip engineering to optimize the plasmon resonance. It is not limited to plexciton control and can be applied to a variety of quantum states ranging from exciton-polariton Bose-Einstein condensates (52) to infrared vibrational resonances (53). Furthermore, it enables active and dynamic control of photochemical pathways in chemically diverse species (54–56) at the single-molecule level.

MATERIALS AND METHODS
Sample preparation
Commercially available CdSe/ZnS QDs (900249-1ML; Sigma-Aldrich) were stabilized with octadecylamine ligands in toluene. The QDs were drop-casted on an Au film coated with Al_2O_3 and blown off by air after 10 to 20 s to avoid aggregation. From AFM imaging, we verified that the density of the QDs on the surface was ~5 dots in a 1 μm by 1 μm window and that they were well dispersed. Atomic layer deposition (ALD) was used to deposit the base and capping layers of Al_2O_3 using trimethylaluminum (TMA) and water as precursors. Depositions were performed in a custom-built flow tube reactor. The base layers were deposited at 200°C, while the capping layers were deposited at 80°C to avoid thermal degradation of the QDs. Depositions occurred under a steady flow of N_2. Each ALD cycle consisted of 0.1 s of TMA pulse, 30 s of N_2 purge, 0.5 s of water pulse, and 30 s of N_2 purge. The growth rates of Al_2O_3 were ~0.1 nm per cycle at 200°C and ~0.08 nm per cycle at 80°C. The number of ALD cycles was adjusted accordingly to achieve the desired dielectric film thickness. The film thickness was confirmed via spectroscopic ellipsometry (alpha-SE, J.A. Woollam) measurements on companion Si wafers.

TESC spectroscopy setup
In the TESC spectroscopy setup, the sample was mounted to a piezoelectric transducer (PZT, P-611.3, Physik Instrumente) with subnanometer precision positioning below an electrically driven and controlled quartz tuning fork (resonance frequency, 32 kHz), which was used to regulate the tip-sample distance using AFM shear-force amplitude feedback (57). Electrochemically etched Au tips (~5- to 10-nm apex radius) were attached to the tuning fork and coarsely positioned using a stepper motor (MX25, Mechonics AG), and shear-force feedback and sample positioning were controlled with a digital AFM controller (R9, RHK Technology). In the TESC spectroscopy setup, the sample was mounted at a 35° angle to the tip axis to maximize the electric field confinement (29). Excitation was provided by a helium-neon laser beam (632.8 nm, ≤1 mW) with a half-wave plate for polarization control that was focused onto the tip-sample interface using an objective lens (numerical aperture, 0.8; LMPLFLN100×; Olympus). PL signal was collected in a backscattering geometry, passed through a dichroic mirror with a 633-nm cutoff, and sent to a spectrometer (f = 500 mm, SpectraPro 500i, Princeton Instruments) with a thermoelectrically cooled, electron-multiplied, charge-coupled device (ProEM+: 1600 eXcelon3, Princeton Instruments). The spectrometer was calibrated using a hydrogen mercury lamp, and a 150 g/mm grating blazed for 800 nm was used to provide high-bandwidth spectral information.

SUPPLEMENTARY MATERIALS
Supplementary material for this article is available at http://advances.sciencemag.org/cgi/content/full/5/7/eaav5931/DC1
Section S1. Characterization of single isolated QDs
Section S2. Lorentzian fitting of emission spectra of uncoupled QD and cavity
Section S3. A coupled oscillator model for plexciton spectra
Section S4. Parameters of model fit
Section S5. FEM simulation of strong coupling
Section S6. FDTD simulation of optical field distribution in a plasmonic cavity
Fig. S1. AFM image of QDs on Au substrate.
Fig. S2. Lorentzian line fit of PL spectra.
Fig. S3. FEM simulation of scattering spectra.
Fig. S4. 3D FDTD simulation of the optical field enhancement.
References (58–60)

REFERENCES AND NOTES
1. J. Claudon, J. Bleuse, N. S. Malik, M. Bazin, P. Jaffrennou, N. Gregersen, C. Sauvan, P. Lalanne, J.-M. Gérard, A highly efficient single-photon source based on a quantum dot in a photonic nanowire. *Nat. Photonics* **4**, 174–177 (2010).
2. C. Kurtsiefer, S. Mayer, P. Zarda, H. Weinfurter, Stable solid-state source of single photons. *Phys. Rev. Lett.* **85**, 290–293 (2000).
3. Y.-M. He, G. Clark, J. R. Schaibley, Y. He, M.-C. Chen, Y.-J. Wei, X. Ding, Q. Zhang, W. Yao, X. Xu, C.-Y. Lu, J.-W. Pan, Single quantum emitters in monolayer semiconductors. *Nat. Nanotechnol.* **10**, 497–502 (2015).
4. C. Palacios-Berraquero, M. Barbone, D. M. Kara, X. Chen, I. Goykhman, D. Yoon, A. K. Ott, J. Beitner, K. Watanabe, T. Taniguchi, A. C. Ferrari, M. Atatüre, Atomically thin quantum light-emitting diodes. *Nat. Commun.* **7**, 12978 (2016).
5. T. Yoshie, A. Scherer, J. Hendrickson, G. Khitrova, H. M. Gibbs, G. Rupper, C. Ell, O. Shchekin, D. Deppe, Vacuum Rabi splitting with a single quantum dot in a photonic crystal nanocavity. *Nature* **432**, 200–203 (2004).
6. J. P. Reithmaier, G. Sek, A. Löffler, C. Hofmann, S. Kuhn, S. Reitzenstein, L. V. Keldysh, V. D. Kulakovskii, T. L. Reinecke, A. Forchel, Strong coupling in a single quantum dot–semiconductor microcavity system. *Nature* **432**, 197–200 (2004).

7. G. Khitrova, H. Gibbs, M. Kira, S. W. Koch, A. Scherer, Vacuum Rabi splitting in semiconductors. *Nat. Phys.* **2**, 81–90 (2006).

8. K. Hennessy, A. Badolato, M. Winger, D. Gerace, M. Atatüre, S. Gulde, S. Fält, E. L. Hu, A. Imamoğlu, Quantum nature of a strongly coupled single quantum dot–cavity system. *Nature* **445**, 896–899 (2007).

9. P. Vasa, W. Wang, R. Pomraenke, M. Lammers, M. Maiuri, C. Manzoni, G. Cerullo, C. Lienau, Real-time observation of ultrafast Rabi oscillations between excitons and plasmons in metal nanostructures with J-aggregates. *Nat. Photonics* **7**, 128–132 (2013).

10. M. Pelton, Modified spontaneous emission in nanophotonic structures. *Nat. Photonics* **9**, 427–435 (2015).

11. P. Bharadwaj, P. Anger, L. Novotny, Nanoplasmonic enhancement of single-molecule fluorescence. *Nanotechnology* **18**, 044017 (2006).

12. J. Seelig, K. Leslie, A. Renn, S. Kühn, V. Jacobsen, M. van de Corput, C. Wyman, V. Sandoghdar, Nanoparticle-induced fluorescence lifetime modification as nanoscopic ruler: Demonstration at the single molecule level. *Nano Lett.* **7**, 685–689 (2007).

13. N. T. Fofang, N. K. Grady, Z. Fan, A. O. Govorov, N. J. Halas, Plexciton dynamics: Exciton- plasmon coupling in a J-aggregate- Au nanoshell complex provides a mechanism for nonlinearity. *Nano Lett.* **11**, 1556–1560 (2011).

14. X.-W. Chen, V. Sandoghdar, M. Agio, Coherent interaction of light with a metallic structure coupled to a single quantum emitter: From superabsorption to cloaking. *Phys. Rev. Lett.* **110**, 153605 (2013).

15. G. Zengin, M. Wersäll, S. Nilsson, T. J. Antosiewicz, M. Käll, T. Shegai, Realizing strong light-matter interactions between single-nanoparticle plasmons and molecular excitons at ambient conditions. *Phys. Rev. Lett.* **114**, 157401 (2015).

16. R. Chikkaraddy, B. de Nijs, F. Benz, S. J. Barrow, O. A. Scherman, E. Rosta, A. Demetriadou, P. Fox, O. Hess, J. J. Baumberg, Single-molecule strong coupling at room temperature in plasmonic nanocavities. *Nature* **535**, 127–130 (2016).

17. D. Melnikau, R. Esteban, D. Savateeva, A. Sánchez-Iglesias, M. Grzelczak, M. K. Schmidt, L. M. Liz-Marzán, J. Aizpurua, Y. P. Rakovich, Rabi splitting in photoluminescence spectra of hybrid systems of gold nanorods and J-aggregates. *J. Phys. Chem. Lett.* **7**, 354–362 (2016).

18. K. Santhosh, O. Bitton, L. Chuntonov, G. Haran, Vacuum Rabi splitting in a plasmonic cavity at the single quantum emitter limit. *Nat. Commun.* **7**, ncomms11823 (2016).

19. R. Liu, Z.-K. Zhou, Y.-C. Yu, T. Zhang, H. Wang, G. Liu, Y. Wei, H. Chen, X.-H. Wang, Strong light-matter interactions in single open plasmonic nanocavities at the quantum optics limit. *Phys. Rev. Lett.* **118**, 237401 (2017).

20. G.-Y. Chen, N. Lambert, C.-H. Chou, Y.-N. Chen, F. Nori, Surface plasmons in a metal nanowire coupled to colloidal quantum dots: Scattering properties and quantum entanglement. *Phys. Rev. B* **84**, 045310 (2011).

21. A. Manjavacas, F. J. García de Abajo, P. Nordlander, Quantum plexcitonics: Strongly interacting plasmons and excitons. *Nano Lett.* **11**, 2318–2323 (2011).

22. H. Leng, B. Szychowski, M.-C. Daniel, M. Pelton, Strong coupling and induced transparency at room temperature with single quantum dots and gap plasmons. *Nat. Commun.* **9**, 4012 (2018).

23. H. Groß, J. M. Hamm, T. Tufarelli, O. Hess, B. Hecht, Near-field strong coupling of single quantum dots. *Sci. Adv.* **4**, eaar4906 (2018).

24. J. M. Atkin, S. Berweger, A. C. Jones, M. B. Raschke, Nano-optical imaging and spectroscopy of order, phases, and domains in complex solids. *Adv. Phys.* **61**, 745–842 (2012).

25. S. Yan, D.-J. Choi, J. A. J. Burgess, S. Rolf-Pissarczyk, S. Loth, Control of quantum magnets by atomic exchange bias. *Nat. Nanotechnol.* **10**, 40–45 (2015).

26. P. Willke, W. Paul, F. D. Natterer, K. Yang, Y. Bae, T. Choi, J. Fernández-Rossier, A. J. Heinrich, C. P. Lutz, Probing quantum coherence in single-atom electron spin resonance. *Sci. Adv.* **4**, eaaq1543 (2018).

27. S. Baumann, W. Paul, T. Choi, C. P. Lutz, A. Ardavan, A. J. Heinrich, Electron paramagnetic resonance of individual atoms on a surface. *Science* **350**, 417–420 (2015).

28. C. Neacsu, G. Steudle, M. Raschke, Plasmonic light scattering from nanoscopic metal tips. *Appl. Phys. B* **80**, 295–300 (2005).

29. K.-D. Park, M. B. Raschke, Polarization control with plasmonic antenna-tips: A universal approach for optical nano-crystallography and vector-field imaging. *Nano Lett.* **18**, 2912–2917 (2018).

30. K.-D. Park, O. Khatib, V. Kravtsov, G. Clark, X. Xu, M. B. Raschke, Hybrid tip-enhanced nanospectroscopy and nanoimaging of monolayer WSe$_2$ with local strain control. *Nano Lett.* **16**, 2621–2627 (2016).

31. V. Kravtsov, S. Berweger, J. M. Atkin, M. B. Raschke, Control of plasmon emission and dynamics at the transition from classical to quantum coupling. *Nano Lett.* **14**, 5270–5275 (2014).

32. T. R. Jensen, M. L. Duval, K. L. Kelly, A. A. Lazarides, G. C. Schatz, R. P. Van Duyne, Nanosphere lithography: Effect of the external dielectric medium on the surface plasmon resonance spectrum of a periodic array of silver nanoparticles. *J. Phys. Chem. B* **103**, 9846–9853 (1999).

33. G. Cui, M. G. Raymer, Emission spectra and quantum efficiency of single-photon sources in the cavity-QED strong-coupling regime. *Phys. Rev. A* **73**, 053807 (2006).

34. F. P. Laussy, E. del Valle, C. Tejedor, Luminescence spectra of quantum dots in microcavities. I. Bosons. *Phys. Rev. B* **79**, 235325 (2009).

35. P. Törmä, W. L. Barnes, Strong coupling between surface plasmon polaritons and emitters: A review. *Rep. Prog. Phys.* **78**, 013901 (2015).

36. A. L. Efros, D. J. Nesbitt, Origin and control of blinking in quantum dots. *Nat. Nanotechnol.* **11**, 661–671 (2016).

37. X. Wu, S. K. Gray, M. Pelton, Quantum-dot-induced transparency in a nanoscale plasmonic resonator. *Opt. Express* **18**, 23633–23645 (2010).

38. S. A. Empedocles, R. Neuhauser, M. G. Bawendi, Three-dimensional orientation measurements of symmetric single chromophores using polarization microscopy. *Nature* **399**, 126–130 (1999).

39. M. L. Andersen, S. Stobbe, A. S. Sørensen, P. Lodahl, Strongly modified plasmon–matter interaction with mesoscopic quantum emitters. *Nat. Phys.* **7**, 215–218 (2011).

40. S. Huang, T. Ming, Y. Lin, X. Ling, Q. Ruan, T. Palacios, J. Wang, M. Dresselhaus, J. Kong, Ultrasmall mode volumes in plasmonic cavities of nanoparticle-on-mirror structures. *Small* **12**, 5190–5199 (2016).

41. S. Jiang, S. Zhang, R. Zhang, C. Hu, M. Liao, Y. Luo, J. Yang, Z. Dong, J. G. Hou, Distinguishing adjacent molecules on a surface using plasmon-enhanced Raman scattering. *Nat. Nanotechnol.* **10**, 865–869 (2015).

42. T. W. Johnson, Z. J. Lapin, R. Beams, N. C. Lindquist, S. G. Rodrigo, L. Novotny, S.-H. Oh, Highly reproducible near-field optical imaging with sub-20-nm resolution based on template-stripped gold pyramids. *ACS Nano* **6**, 9168–9174 (2012).

43. M. Wersäll, J. Cuadra, T. J. Antosiewicz, S. Balci, T. Shegai, Observation of mode splitting in photoluminescence of individual plasmonic nanoparticles strongly coupled to molecular excitons. *Nano Lett.* **17**, 551–558 (2017).

44. A. Reiserer, N. Kalb, G. Rempe, S. Ritter, A quantum gate between a flying optical photon and a single trapped atom. *Nature* **508**, 237–240 (2014).

45. D. Fattal, K. Inoue, J. Vučković, C. Santori, G. S. Solomon, Y. Yamamoto, Entanglement formation and violation of Bell0s inequality with a semiconductor single photon source. *Phys. Rev. Lett.* **92**, 037903 (2004).

46. J. M. Fink, M. Goppl, M. Baur, R. Bianchetti, P. J. Leek, A. Blais, A. Wallraff, Climbing the Jaynes-Cummings ladder and observing its nonlinearity in a cavity QED system. *Nature* **454**, 315–318 (2008).

47. H. U. Yang, R. L. Olmon, K. S. Deryckx, X. G. Xu, H. A. Bechtel, Y. Xu, B. A. Lail, M. B. Raschke, Accessing the optical magnetic near-field through Babinet's principle. *ACS Photonics* **1**, 894–899 (2014).

48. N. Kongsuwan, A. Demetriadou, R. Chikkaraddy, F. Benz, V. A. Turek, U. F. Keyser, J. J. Baumberg, O. Hess, Suppressed quenching and strong-coupling of purcell-enhanced single-molecule emission in plasmonic nanocavities. *ACS Photonics* **5**, 186–191 (2017).

49. M. D. Lukin, A. Imamoğlu, Nonlinear optics and quantum entanglement of ultraslow single photons. *Phys. Rev. Lett.* **84**, 1419–1422 (2000).

50. T. G. Tiecke, J. D. Thompson, N. P. de Leon, L. Liu, V. Vuletić, M. D. Lukin, Nanophotonic quantum phase switch with a single atom. *Nature* **508**, 241 (2014).

51. S. Sun, H. Kim, G. S. Solomon, E. Waks, A quantum phase switch between a single solidstate spin and a photon. *Nat. Nanotechnol.* **11**, 539–544 (2016).

52. J. D. Plumhof, T. Stöferle, L. Mai, U. Scherf, R. F. Mahrt, Room-temperature Bose-Einstein condensation of cavity exciton-polaritons in a polymer. *Nat. Mater.* **13**, 247–252 (2014).

53. E. A. Muller, B. Pollard, H. A. Bechtel, R. Adato, D. Etezadi, H. Altug, M. B. Raschke, Nanoimaging and control of molecular vibrations through electromagnetically induced scattering reaching the strong coupling regime. *ACS Photonics* **5**, 3594–3600 (2018).

54. D. M. Coles, Y. Yang, Y. Wang, R. T. Grant, R. A. Taylor, S. K. Saikin, A. Aspuru-Guzik, D. G. Lidzey, J. K.-H. Tang, J. M. Smith, Strong coupling between chlorosomes of photosynthetic bacteria and a confined optical cavity mode. *Nat. Commun.* **5**, 5561 (2014).

55. A. Shalabney, J. George, J. Hutchison, G. Pupillo, C. Genet, T. W. Ebbesen, Coherent coupling of molecular resonators with a microcavity mode. *Nat. Commun.* **6**, 5981 (2015).

56. J. A. Hutchison, T. Schwartz, C. Genet, E. Devaux, T. W. Ebbesen, Modifying chemical landscapes by coupling to vacuum fields. *Angew. Chem. Int. Ed.* **51**, 1592–1596 (2012).

57. K. Karrai, R. D. Grober, Piezoelectric tip-sample distance control for near field optical microscopes. *Appl. Phys. Lett.* **66**, 1842–1844 (1995).

58. A. D. Rakić, A. B. Djurišić, J. M. Elazar, M. L. Majewski, Optical properties of metallic films for vertical-cavity optoelectronic devices. *Appl. Opt.* **37**, 5271–5283 (1998).

59. R. F. Oulton, V. J. Sorger, T. Zentgraf, R.-M. Ma, C. Gladden, L. Dai, G. Bartal, X. Zhang, Plasmon lasers at deep subwavelength scale. *Nature* **461**, 629–632 (2009).

60. T. P. Sidiropoulos, R. Röder, S. Geburt, O. Hess, S. A. Maier, C. Ronning, R. F. Oulton, Ultrafast plasmonic nanowire lasers near the surface plasmon frequency. *Nat. Phys.* **10**, 870–876 (2014).

Citation: K.-D. Park, M. A. May, H. Leng, J. Wang, J. A. Kropp, T. Gougousi, M. Pelton, M. B. Raschke, Tip-enhanced strong coupling spectroscopy, imaging, and control of a single quantum emitter. *Sci. Adv.* **5**, eaav5931 (2019).